Journal Pre-proof

Gold nanoparticle-mediated bubbles in cancer nanotechnology

Ali Shakeri-Zadeh, Hajar Zareyi, Roghayeh Sheervalilou, Sophie Laurent, Habib Ghaznavi, Hadi Samadian

PII: S0168-3659(20)30746-X

DOI: https://doi.org/10.1016/j.jconrel.2020.12.022

Reference: COREL 10720

To appear in: *Journal of Controlled Release*

Received date: 23 September 2020

Revised date: 11 December 2020

Accepted date: 14 December 2020

Please cite this article as: A. Shakeri-Zadeh, H. Zareyi, R. Sheervalilou, et al., Gold nanoparticle-mediated bubbles in cancer nanotechnology, *Journal of Controlled Release* (2020), https://doi.org/10.1016/j.jconrel.2020.12.022

This is a PDF file of an article that has undergone enhancements after acceptance, such as the addition of a cover page and metadata, and formatting for readability, but it is not yet the definitive version of record. This version will undergo additional copyediting, typesetting and review before it is published in its final form, but we are providing this version to give early visibility of the article. Please note that, during the production process, errors may be discovered which could affect the content, and all legal disclaimers that apply to the journal pertain.

© 2020 Published by Elsevier.

Journal Pre-proof

Gold nanoparticle-mediated bubbles in cancer nanotechnology

Ali Shakeri-Zadeh[1,‡], Hajar Zareyi[2,‡], Roghayeh Sheervalilou[3], Sophie Laurent[4,5], Habib Ghaznavi[3,*], Hadi Samadian[6*]

[1]Finetech in Medicine Research Center, Iran University of Medical Science, Tehran, Iran

[2]Department of Solid State, Faculty of Physics, K.N. Toosi University of Technology, Tehran, Iran

[3]Pharmacology Research Center, Zahedan University of Medical Sciences (ZaUMS), Zahedan, Iran

[4]Laboratory of NMR and Molecular Imaging, University of Mons, Mons B-7000, Belgium

[5]Center for Microscopy and Molecular Imaging (CMMI), Gosselies 6041, Belgium

[6]Nano Drug Delivery Research Center, Health Technology Institute, Kermanshah University of Medical Sciences, Kermanshah, Iran

(*) Corresponding authors:

Habib Ghaznavi, MD, PhD; dr.ghaznavi@zaums.ac.ir

Hadi Samadian, PhD; h3(0)samadiyan@gmail.com

(‡) These authors contributed equally to this work.

Journal Pre-proof

Table of content

Journal Pre-proof

Abstract

Microbubbles (MBs) have been extensively investigated in the field of biomedicine for the past few decades. Ultrasound and laser are the most frequently used sources of energy to produce MBs. Traditional acoustic methods induce MBs with poor localized areas of action. A high level of energy is required to generate MBs through the focused continuous laser, which can be

harmful to healthy tissues. As an alternative, plasmonic light-responsive nanoparticles, such as gold nanoparticles (AuNPs), are preferably used with continuous laser to decrease the energy threshold and reduce the bubbles area of action. It is also well-known that the utilization of the pulsed lasers instead of the continuous lasers decreases the needed AuNPs doses as well as laser power threshold. When well-confined bubbles are generated in biological environments, they play their own unique mechanical and optical roles. The collapse of a bubble can mechanically affect its surrounding area. Such a capability can be used for cargo delivery to cancer cells and cell surgery, destruction, and transfection. Moreover, the excellent ability of light scattering makes the bubbles suitable for cancer imaging. This review firstly provides an overview of the fundamental aspects of AuNPs-mediated bubbles and then their emerging applications in the field of cancer nanotechnology will be reviewed. Although the pre-clinical studies on the AuNP-mediated bubbles have shown promising data, it seems that this technique would not be applicable to every kind of cancer. The clinical application of this technique may basically be limited to the good accessible lesions like the superficial, intracavity and intraluminal tumors. The other essential challenges against the clinical translation of AuNP-mediated bubbles are also discussed.

Key words: Cancer; Nanotechnology; Gold nanoparticles; Bubble; Theranostics.

Journal Pre-proof

Graphical abstract

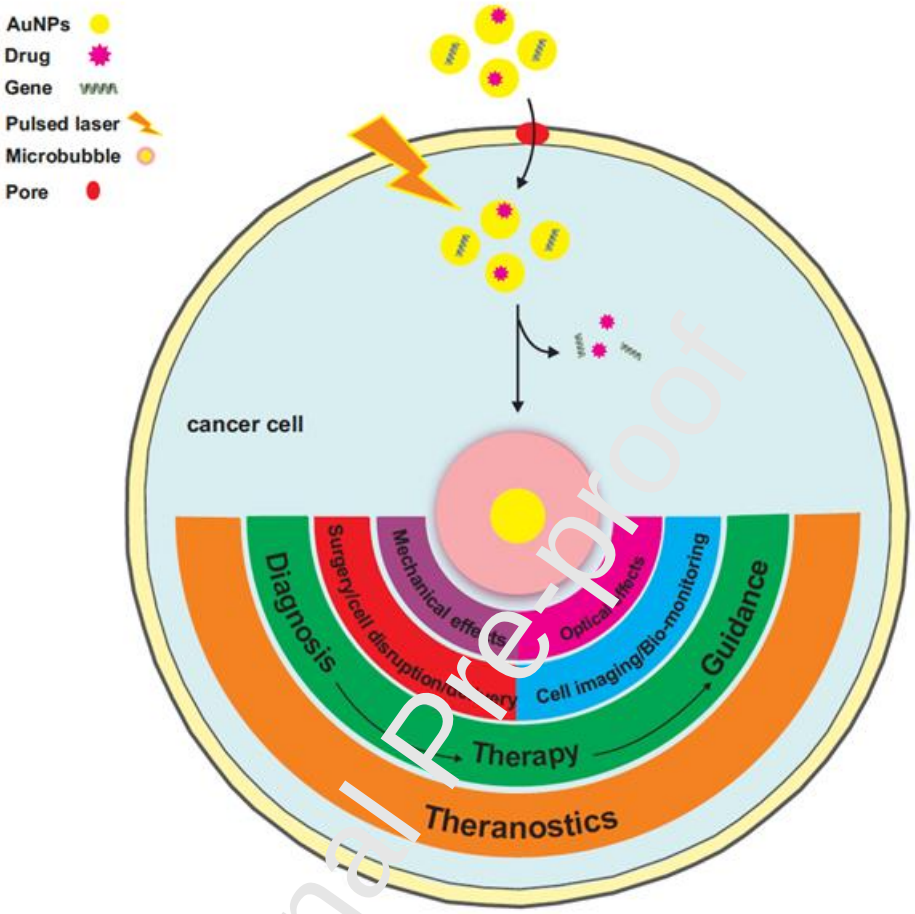

Potential applications of gold nanoparticle-mediated bubbles in cancer nanotechnology

Journal Pre-proof

List of Abbreviations:

Ab: Antibody; **ALG**: Sodium alginate; **AuNP:** Gold (Au) nanoparticle; **AuNRs**: Gold (Au) nanorods; **AuNSs:** Gold (Au) nanoshells; **A431 cell:** Epidermoid carcinoma cell line; **A549 cell:** Lung adenocarcinoma cell; **BT-474 cell:** Human breast carcinoma cell (HER2-positive cells); **BSA:** Bovine serum albumin; **Caco-2 cell:** Epithelial colorectal adenocarcinoma cells; **$CD8^+$ lymphocytes:** cytotoxic T lymphocytes; **Cs:** Chitosan; **CT**: Computed tomography; **Cy7:** Cyanine 7; **C225:** Anti-EGFR Antibody; **Doxil:** Liposome-encapsulated doxorubicin; **EGFR:** Epidermal growth factor receptor; **FBS**: Fetal bovine serum**; FITC-dextran:** Fluorescein isothiocyanate–dextran; **Hep-2C cell:** EGF-positive carcinoma cell; **HEK293T cell:** Immortalized human embryonic kidney cells; **HAuNS:** Hollow Gold (Au) nanoshells; **HNSCC cell:** Head and neck squamous cell carcinoma; **HN31 cell:** Head and neck squamous cell; **HeLa cell**: Immortalized human cervical cancer cells; **H1299 cell**: Human non-small cell lung carcinoma cell; **IgG**: Immunoglobulin G; **i.v.:** Intravenous; **LITT**: Laser-induced thermal therapy; **mAb:** Monoclonal antibody; **MPNS:** Magneto-plasmonic nanoshells; **MDA-MB-231:** Human breast adenocarcinoma cell; **MRI**: Magnetic resonance imaging; **NI**: Not import; **NIR**: Near-infrared; **Panitumumab**: Anti-EGFR Antibody ; **NPs:** Nanoparticles; **NOM9 cell**: Immortalized normal human oral kerot-inocyte cell; **OVCAR-3 cell:** Ovarian carcinoma cell line; **PB:** Plasmonic bubble; **PNBs:** Plasmonic nano bubbles; **PNPs:** Plasmonics Nanoparticles; **PEG:** Polyethylene glycol; **PVP-MPNS:** Polyvinylpyrrolidone-stabilized magneto-plasmonic nanoshells; **pDNA**: Plasmid DNA; **PTT**: Photothermal therapy; **RGCs:** Retinal ganglion cells; **RPE cell:** Human retinal pigment epithelium cell; **siRNA**: Small interfering RNA; **SP:** Surface plasmon; **SNA:** Spherical Nucleic Acid**; ZMTH3 cell**: Adherent canine pleomorphic adenoma cell.

Journal Pre-proof

1. Introduction

Investigations related to the subject of bubbles have been started with acoustic studies. Classical studies on acoustics gave an insight into the theoretical foundations of bubble dynamic physics in the 17th century and then was succeeded by aeroballistics in the 18th century [1]. The study of bubble dynamics and the interaction of bubbles with materials gradually transpired from an inadvertent branch of physics to interdisciplinary sciences. In 1963, it was observed that the focused laser could also generate bubbles in a liquid medium [2]. Many experimental and theoretical studies were performed to understand the underlying mechanisms accurately. It was found that external sources of energies, either ultrasound or laser, are physically able to excite the liquids and produce a localized high pressure and consequently generate dissolved gas in liquids [3]. At the end of this process, bubbles can be created and then they collapse to generate a shock wave.

Generally, there are three traditional methods for micro- and nano-bubble generation (Figure 1): (i) ultrasound irradiation to the liquids [4], (ii) focused continuous laser irradiation to the liquids, and (iii) continuous laser irradiation to the nanoparticles (NPs)-containing liquids [5, 6]. There is also a new method for bubble generation in which a pulsed laser is applied to a liquid medium containing plasmonic NPs (PNPs). In all cases, the generated bubbles (known as transient bubbles with short lifetime) are either in nano or micro size and finally collapse. In biomedicine, the control of bubble size and its mechanical effects are an essential dilemma for using them in precise applications. When an external source of energy is utilized for bubble generation, the locally deposited energy must be lower than the threshold of causing significant damage to the normal tissues. Therefore, all methods of bubble generation, mentioned above, possess their own advantages and disadvantages (as compared in Figure 1).

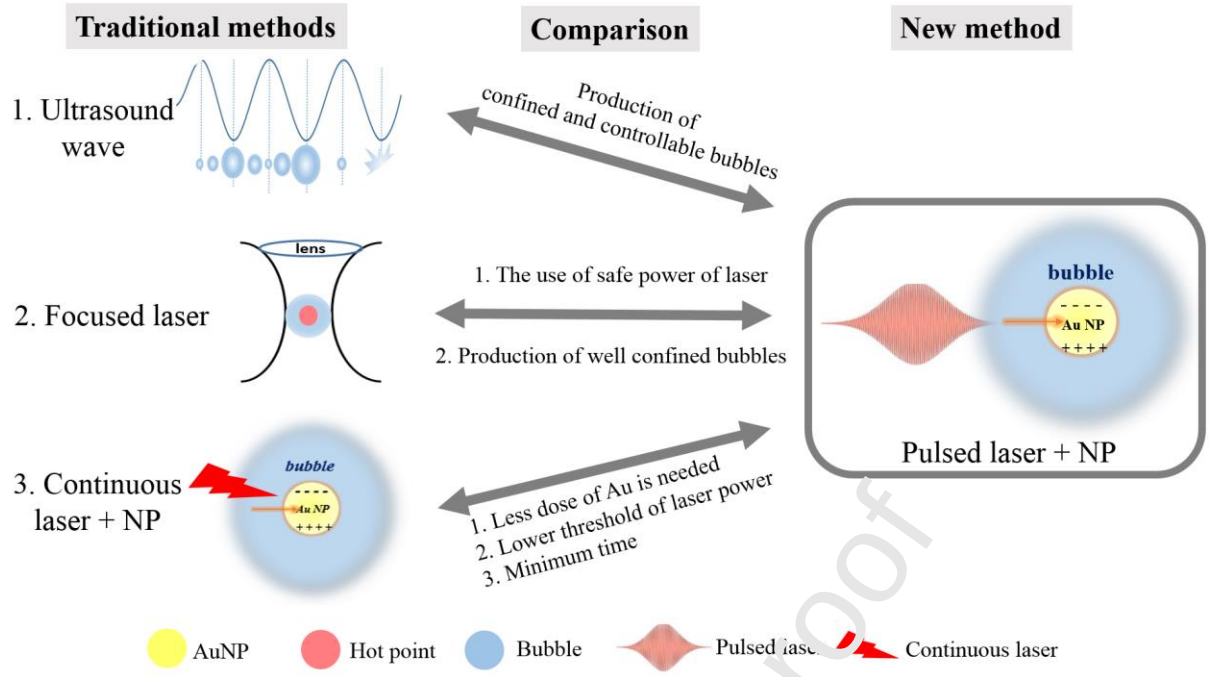

Figure 1. Three traditional methods for micro- and nano-bubble generation and their benefits: (1) ultrasound irradiation to the liquids, (2) focused continuous laser irradiation to the liquids, and (3) continuous laser irradiation to the nanoparticles-containing liquids.

Acoustic methods induce micrometer bubbles with poor localized area of action. The bubble generated through the focused continuous laser may need high energy, damaging the healthy tissues. As an alternative, light-absorbing NPs, such as gold NPS (AuNPs), are preferably used with continuous laser to reduce the energy threshold and action area. On the other hand, it is now well-known that the utilization of the pulsed laser instead of the continuous lasers decreases the needed doses of NPs and reduces the laser power threshold. In this concept, the process of absorbing light by NPs occurs in the range of nano- or pico-seconds, not in a few seconds or minutes. Consequently, significant thermal side effects can be managed when a pulsed laser is utilized instead of continuous lasers.

Journal Pre-proof

In biomedicine, as stated earlier, the most critical challenge is to control the bubble size precisely. One of the best solutions for the confined bubble formation is to use the PNPs [7]. In this situation, the generated bubble is called as the plasmonic nano-bubble (PNB). The effects of the PNBs generated under the interaction of pulsed lasers with PNPs are predominantly mechanical and confined in the bubble area.

When located in biological environments, PNBs play their own unique mechanical and optical roles (Figure 2). The collapse of a bubble can mechanically affect its surrounding area and such a capability can be used for local surgery, cancer cell destruction, transfection and cargo delivery [8]. Moreover, light scattering makes the bubbles suitable for disease imaging and diagnostic applications [9, 10]. The present review intends to summarize the principles of PNB formation and bio-applications of such a kind of bubbles (see also Figure 2 for more details). AuNPs, as the most frequently used agents for PNB generation, are at the focal point of this review article because of having unique optical properties and holding a great promise in various fields of biomedicine such as sensor fabrication, imaging modalities, and photothermal therapy (PTT) of cancer.

Journal Pre-proof

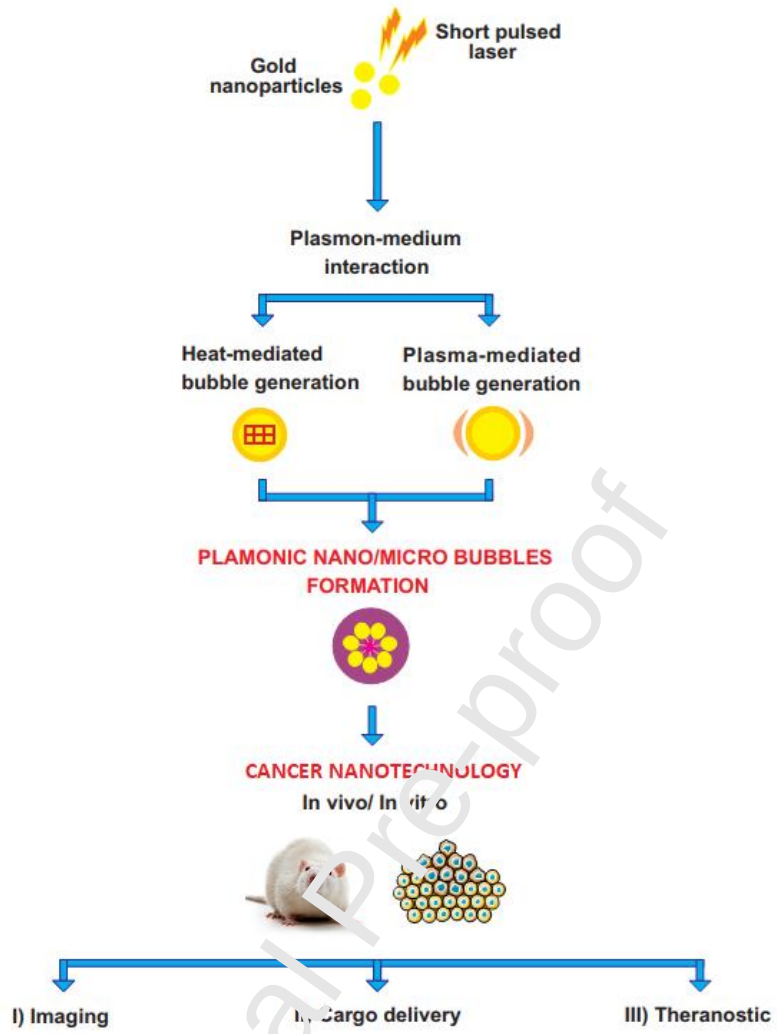

Figure 2. Interaction of AuNPs with short-pulsed laser, two mechanisms of PB formation, and the possible applications of PBs in cancer nanotechnology.

Journal Pre-proof

2. AuNP as a PB generating agent

It is well-known that AuNPs have unique plasmon resonance properties and may absorb the optical energy better than other metallic NPs. Plasmon frequency is related to the coherent electron motion in a confined area, so the geometry and size of AuNPs influence the plasmon frequency [11]. It is well-documented that each size of AuNPs has its own specific absorption spectrum. The maximum absorption of AuNPs with a diameter of 12-41 nm occurs at 520-530 nm [12]. Also, AuNPs are fabricated in various shapes and each shape has its own absorption profile. Interaction of pulsed laser

with AuNPs leads to the production of PNBs [13]. As stated above, AuNP has a high capability for optical energy absorption, making it possible to deposit a high level of energy per confined volume at a picosecond time scale, if AuNPs receive a suitable laser beam. After the interaction of AuNPs and pulsed laser, two processes are probable. In the first process, the local electric field may be strongly enhanced, causing the ionization of AuNPs. Then, as a consequence, the high energetic plasma would be generated in a confined area. The second process is related to the production of a hot point and transferring the energy to the surrounding lactic. These two processes may lead to PNB generation, as explained in Figure 2 [14, 15].

3. Plasmon-medium interaction

The plasmon-medium interaction must be well understood to develop a precise application in biomedical sciences and technologies. In practice, this is an important issue to control the biomedical effects and achieve a unique purpose in biomedicine. When a short laser pulse irradiates AuNPs, they strongly absorb laser energy in a short time (~10^{-12} s) and convert it to heat rapidly due to non-radiative relaxation phenomena [12]. In another possible process, the ionization and deionization occur due to a high local electric field, which highly increases the local area temperature. Figure 3 schematically explains these two possible processes at a glance [16-18].

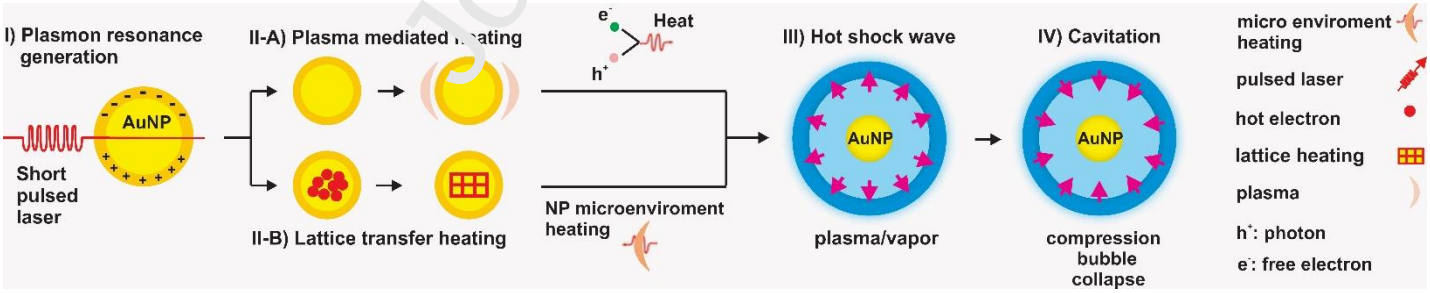

Figure 3. The processes possibly occur right after the interaction of short-pulsed laser with PNPs, like AuNPs. I) interaction of short-pulsed laser with AuNP and generation of surface Plasmon, II-A) plasma-mediated heating, II-B) lattice transfer heating, III) the hot shock wave, and IV) cavitation.

3.1. Heat-mediated PB generation

First of all, it is vital to understand the fundamental physics of the interaction between the pulsed laser with AuNPs and then the underlying physics of PB formation. In this context, it has been demonstrated that appropriate laser light (at the resonance frequency of AuNPs) firstly delivers its energy to the free electrons of AuNPs. Then, the absorbed energy is transferred to the lattice of AuNPs through electron-phonon interactions. Finally, every single AuNP dissipates its energy to the surroundings by thermal diffusion. It is known that such dissipation occurs in the picosecond to nanosecond if the nano-scale particles are used[19, 20].

Bubble formation is quickly initiated if femtosecond and nanosecond lasers are utilized because energy delivery to metal and plasmonic materials is extremely short [21]. The laser-induced heat transfer process with no mass transfer between various kinds of PNPs and the surrounding medium has been modeled in many studies [22, 23]. Here, we review such a process for some typical PNPs. For spherical NPs, the maximum generated temperature can be calculated according to Eq. (1):

$$T = T_{\infty} + \frac{I_0 Q_{abs} r_0}{4K_{\infty}}\left(1 - \exp\left(\frac{3K_{\infty} t_p}{C_0 \rho_0 r_0^2}\right)\right) \quad \text{Eq. (1)}$$

Where T_{∞}, I_0, Q_{abs}, t_p, r_0, K_{∞}, C_0 and ρ_0 are the surrounding tissue temperature, radiation intensity, factor of absorption efficiency, duration of laser pulse, radius of NP, ambient medium thermal conductivity, medium-specific heat capacity and ambient medium density, respectively. Such a calculated temperature (T) can then be used to calculate the final size of the produced bubble [24, 25].

Gold nanoshells (AuNS) are another fascinating and widely used nanostructures for PNBs generation. When AuNSs are used for PNB generation, it is possible to tune the NPs maximum absorption peak by adjusting the shell thickness. In the light of Eq. (1), it is possible to come up with a new equation (Eq. 2) to calculate the heat transfer of AuNSs and their interactions with the surrounding medium:

$$\frac{T-T_\infty}{I_0} = \frac{Q_{abs} r_0}{4K_\infty}\left(1 - \exp\left(\frac{t_p}{\tau_T}\right)\right) \qquad \text{Eq. (2)}$$

$$\tau_T = \frac{r_s^2}{3K_\infty}\left(\frac{C_c \rho_c r_c^3}{r_s^3} + C_s \rho_s \left(1 - \frac{r_c^3}{r_s^3}\right)\right.$$

Where C_c, ρ_c r_c and C_s, ρ_s , r_s are the heat capacity, density and radius of core and shell in the AuNS structure.

It is also possible to have the highest thermal energy by adjusting the laser pulse duration time [21, 26]. As mentioned above, the shape and size of NPs affect their optical and thermal characteristics. For instance, if hollow gold nanoshells (HAuNS) are used, the PNBs generation threshold can be adjusted via controlling the NPs size, shape, and concentration, as well as plasmon resonance frequency [7]. Eq. (3) suggests the way to calculate the maximum temperature dissipated from HAuNS structures [27].

$$\tau_{max} = \frac{\left(\frac{t}{R}\right) 3\rho C_p T_G + \rho_w C_{pw} T_0}{\left(\frac{t}{R}\right) 3\rho\, C_p + \rho_w C_{pw}} \qquad \text{Eq. (3)}$$

Where ρ_w is the density of water and C_{pw} is the heat capacity of water. The ρ, C_p, t and R are the density and heat capacity of HAuNS, shell thickness and radius of HAuNS, respectively. T_G is the Au shell maximum temperature, which induces thermal energy flow leading to the elevation of water temperature and a fall in core temperature until equalization between core-shell and water is attained.

3.2. Plasma-mediated PB generation

There are different ways of bubble generation around PNPs when ultrashort pulses of laser are used. The femtosecond pulses enormously enhance the electric fields around PNPs, leading to the induction of nonlinear absorption of photon energy inside the liquid resulting in plasma generation [28]. The plasma energy is rapidly diffused. Consequently, the pressure and temperature of liquid are quickly increased, leading to bubble generation around PNPs [16]. Plasma formation in liquid via quasi-free electron is described in two mechanisms; photoionization and collision (avalanche)

ionization. Photoionization refers to a phenomenon that is occurred when an electron gets excited by absorbing the photon energy and, consequently, a direct transition from the ground state to a quasi-free state is occurred [29]. For plasma formation by collision (avalanche) ionization, lots of electrons in a transmission medium get highly accelerated by an electric field and collide with other atoms in the medium and subsequently ionize them.

4. PB characteristics and affecting factors

After understanding the mechanism and physics of PB generation, some challenges must be addressed so that the benefits of PB can be thoroughly translated into biomedical fields. Four main issues which must be explored are listed below [27, 30]:

(1) How to control bubble lifetime?

(2) The parameters which determine the maximum bubble size,

(3) The threshold of laser fluence,

(4) Optimum size and concentration of AuNPs for bubble formation.

4.1. Bubble lifetime

Many factors affect the bubble lifetime, such as the size of PNPs, the viscosity of the surrounding medium and the laser parameters. For example, there is a direct correlation between PNPs size and the heat accumulated in the vapor phase of the surrounding liquid, which results in more reduction of the surface tension and medium dynamic viscosity [13]. Such changes allow the initiation of bubble formation and expansion at a lower laser threshold. A bubble may be several micrometers in diameter, and considering the relation of the diameter and lifetime, it may have several microseconds of a lifetime. In a simple method, Eq. (4) is proposed to estimate the bubble lifetime for a continuous laser [31]:

$$\tau_{PNB} = \frac{PK}{6RTD\gamma} a^3 \qquad \text{Eq. (4)}$$

Where P, K, R, T, D, γ and a^3 are ambient pressure, Henry coefficient, gas constant, temperature, laser beam diameter, the surface tension of the liquid/gas interface and the volume of the PB, respectively.

"Fluence" is also one of the most critical factors affecting the bubble lifetime [30]. The more laser fluence and the more optical energy penetrated into PNP, the more lifetime and the larger diameter [32, 33].

4.2. Maximum bubble size

Various methods have been proposed to calculate the radius of bubbles. Rayleigh-Plesset equation is useful for the rising bubble, but it has some limitations regarding the viscosity and tension effects. Recently, another new equation has been presented for a given PNP dispersed in water [34], which is based on the Rayleigh-Plesset and it considers every medium-particle, bubble-particle and bubble-medium thermo-interactions as a function of time:

$$r(t) = \left(\frac{1}{4\pi} \frac{RTC_\infty fP}{MPC_s C_w \rho_w} \left|\frac{dC_s}{dT}\right|\right) t^{1/3} \qquad \text{Eq. (5)}$$

Where R, T, M, P, C_s, C_∞, f, C_w and ρ_w are gas constant, ambient temperature, the molecular mass of the gas, ambient pressure, gas solubility, gas saturation far away from the bubble, heat conversion efficiency, ambient specific heat capacity, and ambient density, respectively [34, 35].

Figure 4. illustrates the bubble dimension regime in different processes of pulsed laser and PNPs interaction. Controlling the size of PNBs enables us to develop several theranostic applications, which will be discussed later.

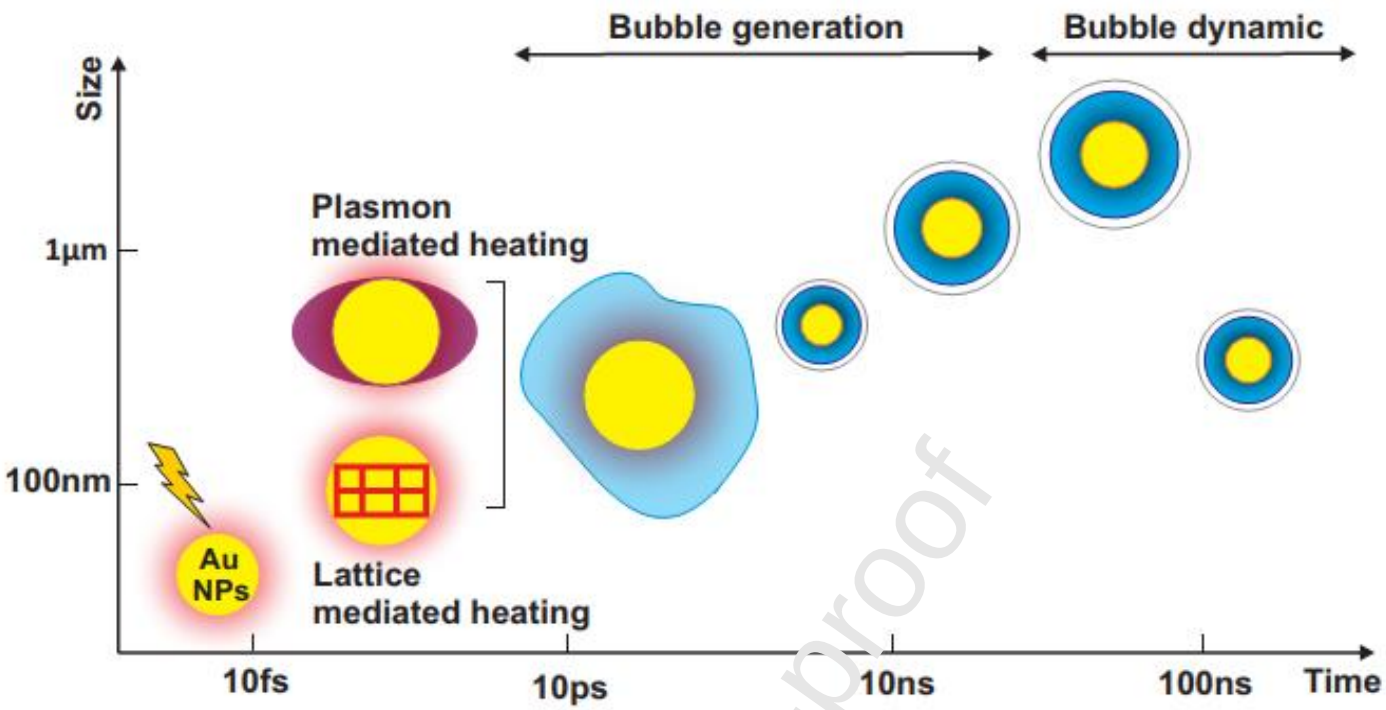

Figure 4. Alteration of time and size of PNBs over a life span of every single bubble.

4.3. Threshold of energy density

Methods of measuring/calculating the threshold of energy density for bubble formation has been theoretically investigated in some studies [24]. Letfullin reported one of the first calculation methods to find threshold intensity for bubble generation as below [36]:

$$I(R) = \frac{4\rho q u_s}{3K_b(R)} \qquad \text{Eq. (6)}$$

Where I, ρ, q, u_s and K_b represent threshold intensity for bubble formation, particle density, particle specific heat, the velocity of bubble rising, which is about the velocity of the acoustic wave in a liquid, and absorption efficiency, respectively. This calculation has clarified that the threshold energy density of ~ 40 mJ/cm^2 is needed for bubble generation if small particles are used, while this amount is ~ 11 mJ/cm^2 if a relatively large particle is used [36]. Some other studies have also shown that the

PNPs and laser properties have effective relations, affecting the bubble properties [37-40]. For more details, we prepared Table 1 summarizing the mentioned concept.

Table 1. Effects of PNPs and laser properties on bubble properties.

NPs shape	NPs concentration (NPs/mL)	NPs size (nm)	Laser setup [λ (nm); t (ps); E (mJ/cm^2)]	Bubble Life span (ns) Max Size (μm)	Ref
HAuNS	1×10^{9}	10 40	[650-100; 28; 1-100]	100 ≤1	[27]
Sphere	1×10^{11}	60	[532; 20-14000; 5]	40 120	[24]
Sphere	2.6×10^{10}	60	[355; 15; 5.2]	10 0.4–0.9	[20]
Rod	4.2×10^{11}	10 × 59	[1064;0.5; 458]	NI 1-5μm	[10]
Sphere	1.7×10^{8}	78	[800; 0.1-5;150-2[illegible]0]	0.1 – 100ns, 0.8 –1 μm	[15]
Sphere	2.4×10^{10}	60	[532; 70, 40]	≥ 200ns 220μm 20-200ns 470μm	[41]

Abbreviations: NPs: Nanoparticles, **HAuNS**: Hollow Gold nanoshells, **NI**: Not informed

4.4. NPs concentration and size

To find out more about the effects of PNPs concentration, it is necessary to determine the optimum distance between PNPs in a single medium. By defining the optical radius, thermal diffusion length, and absorption cross-section for each particle, it is possible to predict the photon-PNP dynamic interactions and the optimum distance between PNPs. Eq. (7) has derived from Rayleigh–Plesset equation and can be used to obtain the interparticle distance [30, 42]:

$$L \leq \sqrt{\left(\frac{2P_{sat}(T_{nuc}) - P_{\infty}}{3\rho(T_{\infty})}\right)\tau_{growth}} \qquad \text{Eq. (7)}$$

where τ_{growth}, T_{nuc}, $P_{sat}(T_{nuc})$, P_{∞} and $\rho(T_{\infty})$ are growth time, nucleation temperature, saturated vapor pressure at the nucleation temperature, ambient pressure, and density of water, respectively. Using the value of interparticle distance, it is possible to estimate the number of required NPs to have a given biomedical effect. For example, it is reported that 430 particles inside a MDA-MB-231 breast cancer cell are required to induce an effective PTT [43].

On the other hand, to find optimum PNP size, the wavelength of scattering and absorption are commonly calculated by Mie theory. It has been suggested that the best size of AuNPs for biomedical applications falls into a range of 10-50 nm. In such a range, the scattering is less than absorption; hence, most of the photon energy would be absorbed, converted to heat, and finally considered as the bubble growing energy [36, 44, 45].

5. Applications of PBs for cancer therapy

5.1. *In vitro* studies

The biomedical applications of PBs have been subjected to various studies due to their promising properties. Pitsillides *et al*. [46] showed that light-absorbing microparticles provide the opportunity to generate tunable microbubbles by optimization of laser fluence. They reported that the generated PBs disrupted cell membrane integrity and induced cell lethality. They also demonstrated that the conjugation of the microparticles with monoclonal anti-human CD8 mouse IgG restricted the lethality to $CD8^+$ T lymphocytes, but not to $CD8^-$ cells. In another study, immunoliposomes containing polyvinylpyrrolidone (PVP)-coated magneto-plasmonic nanoshells (PVP-MPNS) were utilized as cancer therapy agents. They reported that irradiating PVP-MPNS by Ar and 532 nm lasers induced 44.6 and 42.6 % apoptosis in BT-474 human breast carcinoma cell lines, respectively [47]. In another study, Chen *et al.* [48] reported fast and precise single cancer cell damage using gold nanorods (AuNRs) and laser pulse energy as low as ~70 pJ.

A number of comparative studies have been conducted to investigate the effect of particle size on treatment outcomes. One of these studies applied AuNPs with an average size of 30 nm and microparticles with an average size of 0.83 mm and evaluated their toxic effects on $CD8^+$ cells. The authors used 20-ns laser pulses at 532 or 565 nm wavelengths and observed that the NPs were more lethal and exhibited 95% toxicity against cells compared to 80% toxicity induced by the microparticles. Moreover, they reported that the smaller particles induced lower off-target toxicity than the microparticles, stemming from the smaller damage range of the NPs compared to microparticles. They concluded that the size of NPs is critical for effective cancer treatment with the lowest side effect [46]. Researchers have also conducted several theoretical and experimental studies to compare the threshold needed for NPs of different sizes. They applied Mie theory and obtained threshold values of 8.4, 10.4, and 14.0 mJ/cm^2 for particles with diameters of 50 nm, 118 nm, and 200 nm, respectively. The authors reported that the calculated values were 4 times less than the experimental data, around 39 mJ/ cm^2 [49]. Table 2 summarizes the *in vitro* studies conducted on AuNPs-mediated PBs as the cancer therapy projects.

Table 2. *In vitro* studies conducted on AuNPs-mediated PBs as the cancer therapy projects.

NPs size (nm)	Surface coating	Targeting agent	NPs concentration	Cell line	Laser setup [λ (nm); t (ns); E (mJ/cm^2)]	Cell death (%)	Ref
20	BSA	IgG anti-FITC antibody	0.2 (μg/mL)	$CD8^+$ lymphocytes	[532;20;200]	95	[46]
40	-	Goat antimouse IgG	2.4×10^{11} (NPs/mL)	MDA-MB-231	[520; 8; 80]	95	[30]
20	mPEG-SH	C225 Ab	$0.2\text{-}0.6\times10^{11}$ (NPs/mL)	A549 Hep-2C	[532;10;700]	73 93	[38]
60	Doxil	C225 Ab	9×10^{12} (NP/mL)	HN31 NOM9	[780;0.7;40]	≤80	[50]
16	PVP-MPNS,	Herceptin	50 (μg/mL)	BT-474	[532; 8;859]	42.6 cell apoptosis	[47]
60	-	C225 Ab	2.4×10^{10} NPs/mL	HNSCC	[532; 10^{-3}; 40]	≥95	[41]

60	-	Panitumumab	0.7 (μg/mL)	HN31	[782;0.03; 10–66]	Clusters, 10–100-fold higher than single NPs	[51]

Abbreviations: **BSA:** Bovine serum albumin; **NPs:** Nanoparticles; **MDA-MB-231:** Human breast adenocarcinoma cell; **CD8$^+$ lymphocytes:** cytotoxic T lymphocytes; **IgG:** Immunoglobulin G; **Ab:** Antibody; **FITC:** fluorescein isothiocyanate; **Hep-2C:** EGF-positive carcinoma cell; **A549:** Lung adenocarcinoma cell; **HNSCC:** Head and neck squamous cell carcinoma; **HN31:** Head and neck squamous cell; **NOM9:** Immortalized normal human oral kerot-inocyte cell; **BT-474:** Human breast carcinoma cell lines (HER2-positive cells); **PVP-MPNS**: Polyvinylpyrrolidone-coated magneto-plasmonic nanoshells; **C225**: Anti-EGFR Antibody. **Panitumumab:** Anti- epidermal growth factor receptor antibody

5.2. In vivo studies

The combination of pulsed laser and NPs has been applied to destroy skin cancer tissue *in vivo* named as the "laser-activated nano-thermolysis as a cell elimination technology (LANTCET)" [38]. In this technique, researchers applied the microbubbles generated by the interaction of short and ultrashort laser with NPs to detect and eliminate metastasis and residual tumor. They also reported a lifetime above 100 ns for the produced microbubbles. The PNBs have also been utilized to enhance the efficacy of cancer chemotherapy. Some reports show that the therapeutic efficacy of Doxil (liposome-encapsulated doxorubicin) increases from around 7 % to 90% against the head and neck squamous cell carcinoma (HNSCC) in the mouse if PNBs are utilized. In this way, a 20-fold reduction in the Doxil effective dose and 10-fold enhancement in the treatment efficacy using combinatorial therapy compared with chemotherapy alone have been achieved [52].

In addition to conventional cancer therapies, PNBs can be applied to fulfill nanosurgery against microscopic residual diseases. It has been shown that the application of PNBs prevented the local recurrence, providing 100% elimination of tumor cells, and improving survival rate more than two-fold [41, 51, 53, 54]. Shao *et al.* [55] prepared AuNRs-containing folate-conjugated chitosan/sodium alginate microcapsules as the photothermal cancer treatment agent. They applied an 808 nm NIR laser with the fluences of 1.88 J/cm^2, 5.53 J/cm^2, and 9.74 J/cm^2 and observed that the vapor bubbles are generated around the excited capsule. *In vivo* results demonstrated that the fabricated structures could pass through the biological barriers and reach the tumor tissue due to the flexibility in structure and the conjugated folate. The findings showed that the generated microbubbles suppressed tumor

growth and improved PTT efficacy compared to single AuNRs [55-57]. Table 3 summarizes the *in vivo* studies conducted in this concept.

Journal Pre-proof

Table 3. Recent *in vivo* studies conducted on AuNPs-mediated bubbles in the field of cancer therapy. Significant tumor growth inhibition has been reported.

NPs size (nm)	Coating	Targeting agent	Laser setup [λ (nm); t (ns); E (mJ/cm2)]	Cell line /animal	Ref
30	mPEG-SH	Goat anti mouse IgG	[532;10;750]	Rats with pholymorphic sarcoma	[38]
20	-	C225 Ab	[780;0.07;40]	HNSCC xenografted mice	[50]
60	-	C225 Ab	[532;0.001 ,40]	HNSCC xenografted mice	[41]
54	Cy7	Cs/ALG microcapsules	[780;0.07;40]	Mice bearing 4T1 tumors	[55]
60	-	Panitumumab	[782;0.03; 10–20]	HNSCC xenografted mice	[51]
22	sodium silicate shell	Folic acid	[700;5; 20]	mouse ear tissue	[40]
100	-	siRNAs, FITC-dextran	[800;10^{-4}; 111, 229]	RGCs	[58]

Abbreviation: IgG: Immunoglobulin G; **C225 Ab:** Anti-EGFR Antibody; **HNSCC:** Head and neck squamous cell carcinoma; **Cy7:** Cyanine 7; **Cs:** Chitosan; **ALG:** sodium alginate; **Panitumumab:** Anti- epidermal growth factor receptor antibody; **RGCs:** Retinal ganglion cells

6. Imaging with PBs

The application of bubbles as the ultrasonography contrast agent has been originated from the first observation of image contrast enhancement through hand-agitated saline in the 1960s. Microbubbles are currently used as contrast agents in radiology and echocardiography. Small numbers of microbubbles are detectable using an ultrasound system due to their unique acoustic properties originated from their density, compressibility, and harmonic oscillations. Various techniques have been developed for detecting the transient microbubbles in recent decades, including optical and acoustic methods. The optical method includes high-speed photography, scattering methods, dark-

field and pump-probe techniques. Active and passive cavitation detections, and the Doppler method are categorized in the acoustic methods. As multifunctional and sophisticated contrast agents, AuNPs-mediated NBs also offer the additional targeted ability and precise control over the generated bubbles [59-61].

Since the time scale of the bubble collapse is about a few nano- and micro-seconds, imaging techniques with frame rates of at least nano- and micro-seconds are required for monitoring the dynamics of microbubbles activated by pulsed laser [62, 63]. For the time-resolved photothermal imaging of the bubble, a pulse (less than bubble lifetime), or a broad laser beam is irradiated, then a charged-coupled device camera records the data [64]. Optical scattering phenomena provide imaging and monitoring of the PNB dynamics. Moreover, for the detection of transient PNBs with optical methods, some requirements need to be met. For instance, PNB lifetime must be longer than the pulsed illumination within a nano- and pico-second range and the optical pulse should have sufficient energy and precise synchronization of illuminating pulses with the PNB source [65].

The acoustic methods, based on the photoacoustic physics, detect the pressure pulse generated during the generation and collapse of the bubbles. Generally, the acoustic methods are employed for the detection of PNBs in an opaque tissue. Moreover, these methods are low-cost since the optical source and sensors are not required. However, the signal-to-noise ratio and tissue penetration depth for photoacoustic imaging are limited. Using AuNPs, it is possible to improve the sensitivity by increasing the optical absorption and scattering. Table 4 summarizes the studies conducted on AuNPs-mediated bubbles in the field of cancer imagining.

Table 4. Recent studies conducted on AuNPs-mediated bubbles in the field of cancer imaging. Successful tumor detection has been reported.

Imaging modality	Wavelength (nm)	NPs size (nm)	NPs concentration	Bubble life time (ns)	Laser setup [λ (nm); t (ns); E (mJ/cm^2)]	Examined cell line	Ref
Pump-probe scattering	532 575 633	44×16, 25×93, 10×45	-	150-350	[355; 120 ;43] [500; 120 ;43] [350; 120 ;43]	-	[7]
		20 40 60 80 100			[532;500;2200] [532;500;430] [532;500;170] [532;500;120] [532;500;90]		
Pump-probe	535	25	20 (μg/mL)	A few	[535;400000;30]	Caco-2	[66]
Photoacoustic	-	40-50	60 (μg/mL)	A few	[780;15;250]	A431	[26]
Pump-probe dark field	590 -	100	8 (μg/mL)	A few	[800; 45×10^{-6};60-180]	MDA-MB-231	[29]
Acoustic / scattering	- 633	60	0.7 (g/mL)	A few	[782;0.3;70]	HN31	[51]
Scattering	633	60	2.4×10^{10} (NPs/mL)	20-70	[532; NI;45]	HNSCC	[41]
Pump-probe scattering	690 633	50	0.9×10^{11} (NPs/mL)	44	[532,0.5;240]	A549	[67]

Abbreviations: Caco-2: : Epithelial colorectal adenocarcinoma cells**; A431:** Epidermoid carcinoma cell line**; MDA-MB-231:** Human breast adenocarcinoma cell**; HN31:** Head and neck squamous cell**; HNSCC:** Head and neck squamous cell carcinoma**; A549:** Lung adenocarcinoma cell. **NI**: Not informed**. "A few"** means <10 ns.

7. Cargo delivery using PBs

The microbubbles open a new window to the drug delivery area as smart systems, initiating with the collapse near the target site and the release of encapsulated drugs. They can also facilitate drug internalization into the target cells and overcome the dilemma of using high dose drugs due to poor cellular penetration. This method has been actually evaluated for the delivery of both drugs and genes [68, 69]. Figure 5 represents a schematic overview of PB in the field of cargo delivery [70-75].

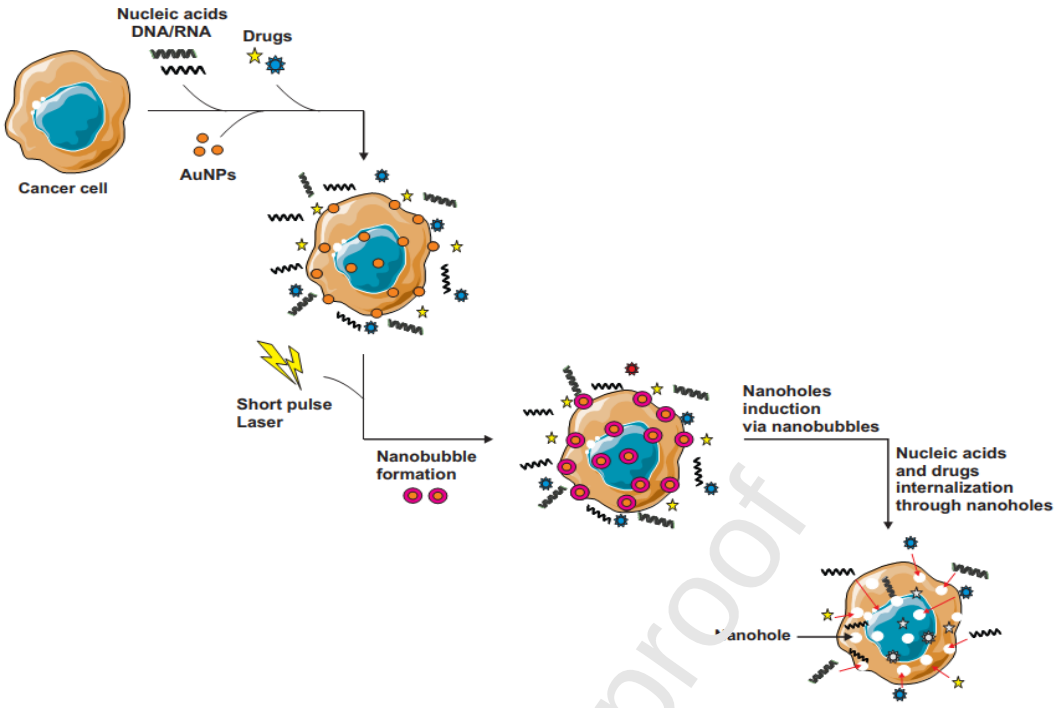

Figure 5. Mechanism of PB-mediated cargo delivery. Nanoholes are generated because of the formation of NBs under interaction of short pulsed. The presence of nanoholes on cell membrane promotes the internalization of drugs or genes.

For gene delivery applications, it is critical to deliver the highest concentration of the genomic materials, as well as to preserve the transfected cells. Ultrasound makes it possible to temporarily increase the permeability of cells and nucleus membranes to deliver the intended amount of DNA/RNA [49, 76, 77]. The application of PNBs can further increase the efficacy of transfection. The effectiveness of transfection can be reached 80-90% *via* controlling the particle size, density, and laser fluence. In a few studies, researchers utilized the combined effects of the interaction of 100 nm AuNPs and 532 nm wavelength laser light as the transfection-enhancing method [77-82]. They reported transfection efficacy of ~75% for the transfection of plasmid DNA into individual mammalian cells. A comparative study reported that spherical AuNPs need 33% more energy and exhibit 61% less efficient than shell structured AuNPs, indicating that shell structured AuNPs have

higher promising potential for cargo delivery [83]. Table 5 summarizes the recent studies conducted on AuNPs-mediated bubbles in the field of cargo delivery.

Table 5. Recent studies conducted on AuNPs-mediated bubbles in the field of cargo delivery.

Cargo	NPs size (nm)	NPs concentration	Laser setup [λ (nm); t (ns); E (mJ/cm2)]	cell line	Delivery efficiency	Ref
Dextran-tetramethylrhodamine, Calcein	118	300 NP/cell	[532; 6; 84]	HeLa	58	[49]
			[532; 6; 36]	HEK293T	98	
FITC-dextran EGFR	30	4×10^3 NPs/cell	[532;4;1500]	OVCAR-3	70	[76]
Antibiotics, FBS	39/28shell 56/15shell	6×10^8 AuNS/cell	[800;0.070;35] [800;0.070;20]	MDA-MB-231	100 90	[84]
FITC-dextran pDNA	200	6.3 μg/cm2	[532;1;80]	ZMTH3	68 57	[85]
FITC-dextrans, siRNA	70	8.2×10^7 NP/mL	[761;7; 2.04×10^3]	HeLa cells, H1299 cells	≥90 >80	[86]
Doxorubicin	AuNRs: 10×59	4.19×10^{11} (NR/mL)	[1064;0.5; 458]	RPE cells, Pig Eyes (*Ex vivo*)	50	[10]

Abbreviations: HeLa cells: Immortalized human cervical cancer cells; **HEK293T:** Immortalized human embryonic kidney cells; **siRNA:** Small interfering RNA; **OVCAR-3:** Ovarian carcinoma cell line; **AuNS:** Au nanoshells; **MDA-MB-231:** Human breast adenocarcinoma cell; **FBS**: Fetal bovine serum; **ZMTH3:** Adherent canine pleomorphic adenoma cell; **FITC-dextran:** Fluorescein isothiocyanate–dextran; **pDNA:** Plasmid DNA; **AuNRs:** Au nanorods. **H1299 cell**: Human non-small cell lung carcinoma cell; **RPE cell**: Human retinal pigment epithelium cell.

8. *Theranostic* methods based on PBs

Another fascinating application of PBs is in the field of theranostics. AuNPs are well-known theranostic agents due to their promising properties, as we recently reviewed elsewhere [87]. Moreover, the combination of transient PBs and PT properties of plasmonic NPs can be a vital component for developing new theranostic agents. AuNPs have their specific diagnostic and treatment possibilities, which can be integrated with contrast enhancement and drug delivery

opportunities of bubbles to develop more efficient theranostic methods. Moreover, the size, mechanical properties, and cargo delivery profile of PBs can be adjusted by controlling both AuNPs properties and laser setup. It has been shown that small size PBs with shorter lifetime fit better for precise diagnostic applications, while medium-size PBs with longer lifetime are more beneficial for the transfection and drug delivery applications. Finally, the biggest size PBs with the longest lifetime are optimal to induce mechanical cell damage and cancer cell destruction [88].

Various studies were conducted to develop sophisticated theranostic agents based on taking advantage of AuNPs-mediated bubbles [40, 88-95]. Lukianova-Hleb *et al.* [14] reported a 50-fold amplification of the optical scattering amplitude, selective and fast damage to specific cells using the combination of 50 nm AuNPs and a 532 nm wavelength pulsed laser irradiation with the duration of 0.5 ns. In another study, Galanzha *et al.* [40] fabricated a 22 nm nanobubble spaser using 10 nm AuNPs with a fluorescent dye-doped silica shell conjugated with folic acid. They reported that the fabricated nanobubble spaser was a super-contrast, multimodal, and ultrafast cellular probe with a single-pulse nanosecond excitation, promising for various *in vitro* and *in vivo* biomedical applications.

9. The clinical opportunities and challenges

Various preclinical studies and clinical trials have been undergoing to evaluate the efficacy and safety of AuNPs-based therapies. For instance, the photothermal cancer therapy effects of silica-AuNSs have recently been investigated and somehow are still being studied in various clinical trials (https://clinicaltrials.gov), like:

- NCT00848042, (2008−2014); for refractory and/or recurrent tumors of the head and neck
- NCT01679470, (2012−2014); for metastatic lung tumors
- NCT02680535, (2016- present); for localized prostate tumors

These clinical trials have been based on the i.v. injections of the NPs and their accumulation into the tumor site based on the passive targeting approach. The photothermal effects of silica-gold AuNSs have also been investigated in other clinical trials for other diseases, like atherosclerosis

(NCT01270139). Another clinical trial study in the field of AuNPs application in cancer therapy has been recently started in Northwestern University (NCT03020017), in which the Spherical Nucleic Acid (SNA) platform's safety and efficacy on recurrent glioblastoma multiforme or gliosarcoma are being investigated. The SNA platform consists of nucleic acids arranged on the surface of small spherical gold nanoparticles.

The biggest challenge against the translation of PNBs into oncology clinics is the low penetration depth of laser light in human tissues, diminishing the general application of this technique in every kind of cancer. This is while the other alternatives for bubble generation in cancer cells can reach much deeper into tissues than laser light. For example, high-frequency ultrasound grants access to deep tissues with good resolution (100 µm lateral and less than 50 µm axial) [96]. However, AuNPs-mediated bubbles induced by laser have shown promising results in the field of cancer therapy over the past two decades, which cannot be easily ignored. As a result, it is necessary to troubleshoot and address this technique's challenges, especially inaccessibility of deap-seated tumors when a laser is used.

The first way to address the penetration depth limitation would be the use of NIR light (750 and 1700 nm) to benefit the first (750 and 1000 nm) and the second (1000 and 1700 nm) biological windows, where the water absorption is minimal [97]. In this way, it would be more possible to deliver light energy to the NPs accumulated in the deep-seated tumors. Although NIR lasers would make the laser energy delivery to deeper tumors a little bit more possible, it still has limitations because depths deeper than 2 cm cannot be effectively exposed by such lasers [98]. Recent advances in optical fiber technology have led to the emergence of the laser-induced thermal therapy (LITT) technique [99]. It is worthy of mentioning this method takes advantage of an optical fiber housed inside a catheter sheath typically used to transmit the laser irradiation from the generator to the desired site in the body. This approach has eliminated the major portion of cancer photothermal therapy limitations and allowed access to deep-seated tumors. Moreover, it is possible to integrate LITT with the imaging modalities such as MRI, ultrasound, CT, and fluoroscopy to precisely locate the optical fiber in the intended location [100, 101].

In practice, LITT is a well-established method and is widely applied to treat various tumors such as gliomas, radiation necrosis, brain tumors, liver metastases, and head and neck cancers. A study conducted on 899 patients with malignant liver tumors treated with MRI–guided LITT over eight years showed that the LITT is safe as an outpatient procedure [102]. Another survey of 381 patients treated with MR-guided LITT resulted in the average survival times of 45.7, 42.7, and 32 months for

patients with liver metastasis, patients with colorectal liver metastases, and for HCC tumors, respectively [103]. The clinical applications of LITT for the treatment of various brain tumors have also been demonstrated. Schwarzmaier *et al.* [104] reported a significant median overall survival time for 16 patients treated with MRI–guided LITT procedure. Another study evaluated the safety and feasibility of MRI–guided LITT for treating patients suffering from resistant focal metastatic intracranial tumors. They reported the treatment of 15 metastatic tumors in 7 patients [105]. Rosenberg *et al.* [106] reported improving patients' long-term survival with pulmonary metastases of the different primary origins, including malignant melanoma colorectal carcinoma, breast carcinoma, renal cell carcinoma, sarcoma, and others. They reported significant elongation in the survival rates when an MRI–guided LITT treatment strategy was applied. These studies all confirm the LITT method's clinical applicability, in which laser light is sometimes delivered to deep-seated tumors. Having looked at promising results reported for such a laser based tumor therapy approach [107-114], it sounds the serious limitations against laser-induced AuNPs-mediated bubbles (as mentioned above) can probably be addressed through taking advantages of optical fiber technology. In this way, the clinical application of AuNPs-mediated bubbles may literally be inflated and intracavity or intraluminal tumors can also be added to the list of accessible cancers.

The long-term toxicity and the biological fate of the AuNPs within human body are the other concerning issues if the AuNPs-mediated PNBs is going to translate into the oncology clinics. Several studies confirmed the biocompatibility of AuNPs. Gad *et al.* conducted comprehensive studies evaluating the long-term toxicity of the i.v. injected AuNSs. They assessed the biodistribution/clearance of AuNSs in mice, the acute and chronic toxicity in Beagle dogs, and the acute toxicity in rats for time durations up to 404 days. They finally ended up reporting that the AuNSs are biocompatible, non-toxic, and well-tolerated [115]. In another study, the safety of AuNSs was evaluated in 22 patients with human prostate cancer and no significant toxicity, no significant immunogenicity, and acceptable tolerance for 6 months were finally reported as the results [116]. Despite these observations, further studies are required to better and more comprehensively address the long-term effects of the AuNPs inside the body. Controversial/contradictory results reported in different toxicological studies is another challenge against the use of AuNPs-mediated bubbles for cancer therapy, which arise from different test models and experiment parameters. Accordingly, developing universal test models is necessary to obtain comparable results and draw a decisive conclusion. Computational modeling and *in silico* techniques, such as quantitative structure-activity relationship (QSAR) [117-120] and artificial neural networks (ANNs) [121-124] approaches may be considered as the proper techniques to address such concerns.

10. Conclusion

Nanotechnology and nanoscience offer innovative and promising possibilities to improve the current imaging and treatment modalities and eliminate their limitations. Microbubbles have exhibited valuable results in imaging and treatment applications while having some drawbacks, such as poor localized areas of action and difficulty in controlling their physical and mechanical properties. The bubbles generated through the focused continuous laser may need high energy, damaging the healthy tissues. Utilizing plasmonic NPs, such as AuNPs as the energy transferring agent, provides the ability to apply lower energy to form the bubbles. When we generate the AuNPs-mediated bubbles using a laser pulse, we need lower amout of NPs in comparison to the other nanotechnology-based diagnostic and treatment modalities. The AuNPs-mediated bubbles are multi-functional, tunable, and on-demand theranostic agents, which will not emerge in AuNPs-free tissues. The use of such bubbles provides good control over the bubbles physicomechanical properties and enough precision at the location of AuNPs. Also, we would be able to remotely control and activate the AuNPs by a laser pulse and dynamically tune with the energy of laser pulses. Moreover, it is possible to control the bubble's mechanical and optical properties by adjusting the AuNPs' characteristics. Through such an adjustment, minimum off-target destructive damage would be achievable. Today, we know that small size PBs with shorter lifetime are good tools for precise diagnostic applications, while medium-size PBs with longer lifetime are more beneficial for transfection and drug delivery applications. Moreover, the biggest size PBs with the longest lifetime are optimal to induce mechanical cell damage and cancer cell destruction. Certainly, targeting of the AuNPs with proper and cancer-specific biomarkers would enhance the diagnosis/therapy efficacy of AuNPs-mediated bubbles. Along with listing the beneficial advantages of AuNPs-mediated bubbles, it should be mentioned that there are still some sever challenges against the clinical translation of this technology,

as discussed in section 9, needing to be addressed well so as to accelerate the clinical translation process.

Acknowledgments

The authors gratefully acknowledge the supports received from Zahedan University of Medical Sciences and Kermanshah University of Medical Sciences.

Competing interests

The authors declare no competing financial interest.

Journal Pre-proof

References

[1] M.S. Plesset, A. Prosperetti, Bubble dynamics and cavitation, Annual review of fluid mechanics, 9 (1977) 145-185.

[2] G. Askar'yan, A. Prokhorov, G. Chanturiya, G. Shipulo, The effects of a laser beam in a liquid, Sov. Phys. JETP, 17 (1963) 1463-1465.

[3] F.R. Gilmore, The growth or collapse of a spherical bubble in a viscous compressible liquid, (1952).

[4] M. Alheshibri, J. Qian, M. Jehannin, V.S. Craig, A history of nanobubbles, Langmuir, 32 (2016) 11086-11100.

[5] O. Angelsky, A.Y. Bekshaev, P. Maksimyak, A. Maksimyak, S.G. Hanson, S. Kontush, Controllable generation and manipulation of micro-bubbles in water with absorptive colloid particles by CW laser radiation, Optics express, 25 (2017) 5232-5243.

[6] M.L. Leclair, Method and apparatus for the controlled formation of cavitation bubbles, in, Google Patents, 2005.

[7] A.M. Fales, W.C. Vogt, K.A. Wear, T.J. Pfefer, I.K. Ilev, Experimental investigation of parameters influencing plasmonic nanoparticle-mediated bubble generation with nanosecond laser pulses, Journal of biomedical optics, 24 (2019) 065003.

[8] B. Dollet, P. Marmottant, V. Garbin, Bubble dynamics in soft and biological matter, Annual Review of Fluid Mechanics, 51 (2019) 331-355.

[9] D.O. Lapotko, K. Hleb, Diagnosis, removal, or mechanical damaging of tumor using plasmonic nanobubbles, in, Google Patents, 2019.

[10] Z. Zhang, M. Taylor, C. Collins, S. Haworth, Z. Shi, Z. Yuan, X. He, Z. Cao, Y.C. Park, Light-Activatable Theranostic Agents for Image-Monitored Controlled Drug Delivery ,ACS applied materials & interfaces, 10 (2018) 1534-1543.

[11] H. Zareyi, M. Vaezzadeh, Geometry Effect on Plasmon Frequency in Triangular Nanoprism, Plasmonics, 13 (2018) 1759-1765.

[12] S. Link, M.A. El-Sayed, Size and temperature dependence of the plasmon absorption of colloidal gold nanoparticles, The Journal of Physical Chemistry B, 103 (1999) 4212-4217.

[13] D. Lapotko, Plasmonic nanoparticle-generated photothermal bubbles and their biomedical applications, Nanomedicine, 4 (2009) 813-845.

[14] E. Lukianova-Hleb, E. Hanna, J. Hafner, D. Lapotko, Tunable plasmonic nanobubbles for cell theranostics, Nanotechnology, 21 (2010) 085102.

[15] A. Dagallier, E. Boulais, C. Boutopoulos, R. Lachaine, M. Meunier, Multiscale modeling of plasmonic enhanced energy transfer and cavitation around laser-excited nanoparticles, Nanoscale, 9 (2017) 3023-3032.

[16] A. Vogel, J. Noack, G. Hüttman, G. Paltauf, Femtosecond plasma-mediated nanosurgery of cells and tissues, in: Laser Ablation and its Applications, Springer, (2007) 231-280.

[17] R.m. Lachaine, E.t. Boulais, M. Meunier, From thermo-to plasma-mediated ultrafast laser-induced plasmonic nanobubbles, Acs Photonics, 1 (2014) 331-336.

[18] S. Hashimoto, T. Katayama, K. Setoura, M. Strasser, T. Uwada, H. Miyasaka, Laser-driven phase transitions in aqueous colloidal gold nanoparticles under high pressure: picosecond pump–probe study, Physical Chemistry Chemical Physics, 18 (2016) 4994-5004.

[19] W. Huang, W. Qian, M.A. El-Sayed, Y. Ding, Z.L. Wang, Effect of the lattice crystallinity on the electron− phonon relaxation rates in gold nanoparticles, The Journal of Physical Chemistry C, 111 (2007) 10751-10757.

[20] T. Katayama, K. Setoura, D. Werner, H. Miyasaka, S. Hashimoto, Picosecond-to-nanosecond dynamics of plasmonic nanobubbles from pump–probe spectral measurements of aqueous colloidal gold nanoparticles, Langmuir, 30 (2014) 9504-9513.

[21] K. Metwally, S. Mensah, G. Baffou, Fluence threshold for photothermal bubble generation using plasmonic nanoparticles, The Journal of Physical Chemistry C, 119 (2015) 28586-28596.

[22] V. Pustovalov, A. Smetannikov, V. Zharov, Photothermal and accompanied phenomena of selective nanophotothermolysis with gold nanoparticles and laser pulses, Laser Physics Letters, 5 (2008) 775.

[23] V. Pustovalov, L. Astafyeva, B. Jean, Computer modeling of the optical properties and heating of spherical gold and silica-gold nanoparticles for laser combined imaging and photothermal treatment, Nanotechnology, 20 (2009) 225105.

[24] E.Y. Lukianova-Hleb, A.N. Volkov, D.O. Lapotko, Laser pulse duration is critical for the generation of plasmonic nanobubbles, Langmuir, 30 (2014) 7425-7434.

[25] T. Wu, C.H. Farny, R.A. Roy, R. Holt, Modeling cavitation nucleation from laser-illuminated nanoparticles subjected to acoustic stress, The Journal of the Acoustical Society of America, 130 (2011) 3252-3263.

[26] G. Ku, Q. Huang, X. Wen, J. Ye, D. Piwnica-Worms, C. Li, Spatial and Temporal Confined Photothermolysis of Cancer Cells Mediated by Hollow Gold Nanospheres Targeted to Epidermal Growth Factor Receptors, ACS omega, 3 (2018) 5888-5895.

[27] M.O. Ogunyankin, J.E. Shin, D.O. Lapotko, V.E. Ferry, J.A. Zasadzinski, Optimizing the NIR fluence threshold for nanobubble generation by controlled synthesis of 10–40nm hollow gold nanoshells, Advanced Functional Materials, 28 (2018) 1705272.

[28] E.t. Boulais, R.m. Lachaine, M. Meunier, Plasma-mediated nanocavitation and photothermal effects in ultrafast laser irradiation of gold nanorods in water, The Journal of Physical Chemistry C, 117 (2013) 9386-9396.

[29] C. Boutopoulos, E. Bergeron, M. Meunier, Cell perforation mediated by plasmonic bubbles generated by a single near infrared femtosecond laser pulse, Journal of biophotonics, 9 (2016) 26-31.

[30] V. Zharov, R .Letfullin, E. Galitovskaya, Microbubbles-overlapping mode for laser killing of cancer cells with absorbing nanoparticle clusters, Journal of Physics D: Applied Physics, 38 (2005) 2571.

[31] G. Baffou, J. Polleux, H. Rigneault, S. Monneret, Super-heating and micro-bubble generation around plasmonic nanoparticles under cw illumination, The Journal of Physical Chemistry C, 118 (2014) 4890-4898.

[32] R.R. Letfullin, T.F. George, Computational Nanomedicine and Nanotechnology: lectures with computer practicums, Springer, 2017.

[33] D. Lapotko, Plasmonic nanobubbles as tunable cellular probes for cancer theranostics, Cancers, 3 (2011) 802-840.

[34] C.E. Brennen, Cavitation and bubble dynamics, Cambridge University Press, 2014.

[35] Y. Wang, M.E. Zaytsev, H.L .The, J.C. Eijkel, H.J. Zandvliet, X. Zhang, D. Lohse, Vapor and gas-bubble growth dynamics around laser-irradiated, water-immersed plasmonic nanoparticles, ACS nano, 11 (2017) 2045-2051.

[36] R. Letfullin, C. Joenathan, T. George, V. Zharov, Cancer cell killing by laser-induced thermal explosion of nanoparticles, Nanomedicine, 1 (2006) 473-480.

[37] G. Akchurin, B. Khlebtsov, G. Akchurin, V. Tuchin, V. Zharov, N. Khlebtsov, Gold nanoshell photomodification under a single-nanosecond laser pulse accompanied by color-shifting and bubble formation phenomena, Nanotechnology, 19 (2007) 015701.

[38] E.Y. Hleb, J.H. Hafner, J.N. Myers, E.Y. Hanna, B.C. Rostro, S.A. Zhdanok, D.O. Lapotko, LANTCET: elimination of solid tumor cells with photothermal bubbles generated around clusters of gold nanoparticles, Nanomedicien, 3 (2008) 647-667.

[39] N. Katchinskiy, R. Godbout, A. Hatef, A. Elezzabi, Anti-EpCAM Gold Nanorods and Femtosecond Laser Pulses for Targeted Lysis of Retinoblastoma, Advanced Therapeutics, 1 (2018) 1800009.

[40] E.I. Galanzha, R. Weingold, D.A. Nedosekin, M. Sarimollaoglu, J. Nolan, W. Harrington, A.S. Kuchyanov, R.G. Parkhomenko, F. Watanabe, Z. Nima, Spaser as a biological probe, Nature communications, 8 (2017) 15528.

[41] E.Y. Lukianova-Hleb, Y. Kim, R.R. Sawant, X. Wu ,V.P. Torchilin, D.O. Lapotko, On-demand intracellular amplification of chemoradiation with cancer-specific plasmonic nanobubbles, Nature medicine, 20 (2014) 778.

[42] V.P. Zharov, V. Galitovsky, P. Chowdhury, T. Chambers, Photothermal evaluation of the influence of nicotine, antitumor drugs, and radiation on cellular absorbing structures, in: Photons Plus Ultrasound: Imaging and Sensing, International Society for Optics and Photonics, 2004, pp. 196-207.

[43] X. Hou, N. Djellali, B. Palpant, Absorption of ultrashort laser pulses by plasmonic nanoparticles: not necessarily what you might think, ACS Photonics, 5 (2018) 3856-3863.

[44] R.R. Letfullin, C. Joenathan, T.F. George, V.P. Zharov, Laser-induced explosion of gold nanoparticles: potential role for nanophotothermolysis of cancer, Nanomedicien, 1 (2006): 473-480.

[45] V.P. Zharov, J.-W. Kim, D.T. Curiel, M. Everts, Self-assembling nanoclusters in living systems: application for integrated photothermal nanodiagnostics and nanotherapy, Nanomedicine: Nanotechnology, Biology and Medicine, 1 (2005) 326-345.

[46] C.M. Pitsillides, E.K. Joe, X. Wei, R.R. Anderson, C.P. Lin, Selective cell targeting with light-absorbing microparticles and nanoparticles, Biophysical journal, 84 (2003) 4023-4032.

[47] M.E. Khosroshahi, Z. Hassannejad ,M. Firouzi, A.R. Arshi, Nanoshell-mediated targeted photothermal therapy of HER2 human breast cancer cells using pulsed and continuous wave lasers: an in vitro study, Lasers in medical science, 30 (2015) 1913-1922.

[48] Z. Chen, H. Fan, J. Li, S. Tie, S .Lan, Photothermal therapy of single cancer cells mediated by naturally created gold nanorod clusters, Optics express, 25 (2017) 15093-15107.

[49] T.-H. Wu, S. Kalim, C. Callahan, M.A. Teitell, P.-Y. Chiou, Image patterned molecular delivery into live cells using gold particle coated substrates, Optics express, 18 (2010) 938-946.

[50] E.Y. Lukianova-Hleb, Ren, Xiaoyang, Townley, Debra, et al.. " . , Plasmonic Nanobubbles Rapidly Detect and Destroy Drug-Resistant Tumors." Theranostics, , 2, (2012) 976-987.

[51] E.Y. Lukianova-Hleb, Y.-S. Kim, I. Belatsarkouski, A.M. Gillenwater, B.E. O'Neill, D.O. Lapotko, Intraoperative diagnostics and elimination of residual microtumours with plasmonic nanobubbles, Nature nanotechnology, 11 (2016) 525.

[52] E.Y. Lukianova-Hleb, X. Ren, D. Townley, X. Wu, M.E. Kupferman, D.O. Lapotko, Plasmonic nanobubbles rapidly detect and destroy drug-resistant tumors, Theranostics, 2 (2012) 976.

[53] A.P. Jathoul, J. Laufer, O. Ogunlade, B. Treeby, B. Cox, E. Zhang, P. Johnson, A.R .Pizzey, B. Philip, T. Marafioti, Deep in vivo photoacoustic imaging of mammalian tissues using a tyrosinase-based genetic reporter, Nature Photonics, 9 (2015) 239.

[54] M.S. Hutson, X. Ma, Plasma and cavitation dynamics during pulsed laser microsurgery in vivo, Physical review letters, 99 (2007) 158104.

[55] J. Shao, M. Xuan, L. Dai, T. Si, J. Li, Q. He, Near-Infrared-Activated Nanocalorifiers in Microcapsules: Vapor Bubble Generation for In Vivo Enhanced Cancer Therapy, Angewandte Chemie International Edition, 54 (2015) 12782-12787.

[56] R. Popovtzer, A. Agrawal, N.A. Kotov, A. Popovtzer, J. Balter, T.E. Carey, R. Kopelman, Targeted gold nanoparticles enable molecular CT imaging of cancer, Nano letters, 8 (2008) 4593-4596.

[57] A. Kharlamov, A. Tyurnina ,V. Veselova, O. Novoselova, A. Filatova, O. Kovtun, Plasmonics for treatment of atherosclerosis: results of NANOM-FIM trial, J Nanomed Nanotechol, 4 (2013) 2.

[58] A.M. Wilson, J. Mazzaferri, E. Bergeron, S. Patskovsky, P. Marcoux-Valiquette, S. Costantino, P. Sapieha, M. Meunier, in vivo laser-mediated retinal ganglion cell optoporation using KV1. 1 conjugated gold nanoparticles, Nano letters, 18 (2018) 6981-6988.

[59] M. Mahmoudi, V. Serpooshan, S. Laurent, Engineered nanoparticles for biomolecular imaging, Nanoscale, 3 (2011) 3007-3026.

[60] A. Lahooti, S. Sarkar, S. Laurent, S. Shanehsazzadeh, Dual nano-sized contrast agents in PET/MRI: a systematic review, Contrast media & molecular imaging, 11 (2016) 428-447.

[61] Y.-X.J. Wáng, Y. Choi, Z. Chen, S .Laurent, S.L. Gibbs, Molecular imaging: from bench to clinic, BioMed research international, 2014 (2014.(

[62] M. Mozneb, A.M. Mirza, C.-Z. Li, Non-Invasive Plasmonic Based Real Time Characterization of Cardiac Drugs on Cardiomyocytes Functional Behavior, Analytical Chemistry, 2 (2019): 2244-2250.

[63] L. Lin, X. Peng, M. Wang, L. Scarabelli, Z. Mao, L.M. Liz-Marzán, M.F. Becker, Y. Zheng, Light-directed reversible assembly of plasmonic nanoparticles using plasmon-enhanced thermophoresis, ACS nano, 10 (2016) 9659-9668

[64] D. Lapotko, L. Heat, Laser photothermal microscopy for functional imaging of live cells, Microscopy, (2013) 27-29.

[65] E.Y. Lukianova-Hleb, D.O. Lapotko, Plasmonic Nanobubbles for Cancer Theranostics, in: Engineering in Translational Medicine, Springer, 2014, pp. 879-926.

[66] A. Becker, T. Lehrich, S. Kalies, A. Heisterkamp, A. Ngezahayo, Parameters for Optoperforation-Induced Killing of Cancer Cells Using Gold Nanoparticles Functionalized With the C-terminal Fragment of Clostridium Perfringens Enterotoxin, International journal of molecular sciences, 20 (2019) 4248.

[67] E. Lukianova-Hleb, E.Y. Hanna, J. Hafner, D. Lapotko, Corrigendum: Tunable plasmonic nanobubbles for cell theranostics (2010 Nanotechnology 21 085102), Nanotechnology, 21 (2010) 085102

[68] W.G. Pitt, G.A. Husseini, B.J. Staples, Ultrasonic drug delivery—a general review, Expert opinion on drug delivery, 1 (2004) 37-56.

[69] M. Mozafari, M. Shimoda, A.M. Urbanska, S. Laurent, Ultrasound-targeted microbubble destruction: toward a new strategy for diabetes treatment, Drug discovery today, 21 (2016) 540-543.

[70] K. Cho, X. Wang, S. Nie, D.M. Shin, Therapeutic nanoparticles for drug delivery in cancer, Clinical cancer research, 14 (2008) 1310-1316.

[71] H. Yuan, A.M. Fales, T. Vo-Dinh, TAT peptide-functionalized gold nanostars: enhanced intracellular delivery and efficient NIR photothermal therapy using ultralow irradiance, Journal of the American Chemical Society, 134 (2012) 11358-11361.

[72] D.S. Wagner, N.A. Delk, E.Y. Lukianova-Hleb, J.H. Hafner, M.C. Farach-Carson, D.O. Lapotko, The in vivo performance of plasmonic nanobubbles as cell theranostic agents in zebrafish hosting prostate cancer xenografts, Biomaterials, 31 (2010) 7567-7574.

[73] L.J. Anderson, E. Hansen, E.Y. Lukianova-Hleb, J.H. Hafner, D.O. Lapotko, Optically guided controlled release from liposomes with tunable plasmonic nanobubbles, Journal of Controlled Release, 144 (2010) 151-158.

[74] Y. Lee, Formulation of Controlled Liposomal Drug Delivery System, in, Purdue University, 2017.

[75] F. Tantussi, G.C. Messina, R. Capozza, M. Dipalo, L. Lovato, F. De Angelis, Long-Range Capture and Delivery of Water-Dispersed Nano-objects by Microbubbles Generated on 3D Plasmonic Surfaces, ACS nano 12.5 (2018): 4116-4122.

[76] C. Yao, F. Rudnitzki, G. Hüttmann, Z. Zhang, R. Rahmanzadeh, Important factors for cell-membrane permeabilization by gold nanoparticles activated by nanosecond-laser irradiation, International journal of nanomedicine, 12 (2017) 5659-5672.

[77] Y. Arita, M. Ploschner, M .Antkowiak, F. Gunn-Moore, K. Dholakia, Laser-induced breakdown of an optically trapped gold nanoparticle for single cell transfection, Optics letters, 38 (2013) 3402-3405.

[78] B. Will, U. Steidl, Multi-parameter fluorescence-activated cell sorting and analysis of stem and progenitor cells in myeloid malignancies, Best Practice & Research Clinical Haematology, 23 (2010) 391-401.

[79] S. Rutella, C. Rumi, L. Laurenti, L. Pierelli, F. Sora', S. Sica, G. Leone, Immune reconstitution after transplantation of autologous peripheral CD34+ cells: analysis of predictive factors and comparison with unselected progenitor transplants, British journal of haematology, 108 (2000) 105-115.

[80] T. Mars, M. Strazisar, K. Mis, N. Kotnik, K. Pegan, J. Lojk, Z. Grubic, M. Pavlin, Electrotransfection and lipofection show comparable efficiency for in vitro gene delivery of primary human myoblasts, The Journal of membrane biology, 248 (2015) 273-283.

[81] E.Y. Lukianova-Hleb, A.P. Samaniego, J. Wen, L.S. Metelitsa, C.-C. Chang ,D.O. Lapotko, Selective gene transfection of individual cells in vitro with plasmonic nanobubbles, Journal of controlled release, 152 (2011) 286-293.

[82] S. Mura, J. Nicolas, P. Couvreur, Stimuli-responsive nanocarriers for drug delivery, Nature materials, 12 (2013) 991.

[83] R. Lachaine, C. Boutopoulos, P.-Y. Lajoie, E.t. Boulais, M. Meunier, Rational design of plasmonic nanoparticles for enhanced cavitation and cell perforation, Nano letters, 16 (2016) 3187-3194.

[84] R.m. Lachaine, C. Boutopoulos, P-.Y. Lajoie, E.t. Boulais, M. Meunier, Rational design of plasmonic nanoparticles for enhanced cavitation and cell perforation. Nano letters, 16 (2016) 3187-3194.

[85] M. Schomaker, D. Killian, S. Willenbrock, D. Heinemann, S. Kalies, A. Ngezahayo, I. Nolte, T. Ripken, C. Junghanß, H. Meyer, Biophysical effects in off-resonant gold nanoparticle mediated (GNOME) laser transfection of cell lines, primary-and stem cells using fs laser pulses, Journal of biophotonics, 8 (2015) 646-658.

[86] R. Xiong, K. Raemdonck, K. Peynshaert, I. Lentacker, I. De Cock, J. Demeester, S.C. De Smedt, A.G. Skirtach, K. Braeckmans, Comparison of gold nanoparticle mediated photoporation: vapor nanobubbles outperform direct heating for delivering macromolecules in live cells, ACS nano, 8 (2014) 6288-6296.

[87] J. Beik, M. Khateri, Z. Khosravi, S.K. Kamrava, S. Kooranifar, H. Ghaznavi, A. Shakeri-Zadeh, Gold nanoparticles in combinatorial cancer therapy strategies, Coordination Chemistry Reviews, 387 (2019) 299-324.

[88] E.Y. Lukianova-Hleb, E.S. Yvon, E.J. Shpall, D.O. Lapotko, All-in-one processing of heterogeneous human cell grafts for gene and cell therapy, Molecular Therapy-Methods & Clinical Development, 3 (2016) 16012.

[89] T. Curry, R. Kopelman, M. Shilo, R. Popovtzer, Multifunctional theranostic gold nanoparticles for targeted CT imaging and photothermal therapy, Contrast media & molecular imaging, 9 (2014) 53-61.

[90] A.K. Parchur, G. Sharma, J.M. Jagtap, V.R. Gogineni, P.S. LaViolette, M.J. Flister, S.B. White, A. Joshi, Vascular Interventional Radiology-Guided Photothermal Therapy of Colorectal Cancer Liver Metastasis with Theranostic Gold Nanorods, ACS nano, 12 (2018) 6597-6611.

[91] T. Dreifuss, E. Barnoy, M. Motiei, R. Popovtzer, Theranostic gold nanoparticles for CT imaging, in: Design and Applications of Nanoparticles in Biomedical Imaging, Springer, 2017, pp. 403-427.

[92] X. Huang, P.K. Jain, I.H. El-Sayed, M.A. El-Sayed, Gold nanoparticles: interesting optical properties and recent applications in cancer diagnostics and therapy, (2007) 681-693.

[93] I. Karampelas, Computational analysis of pulsed-laser plasmon-enhanced photothermal energy conversion and nanobubble generation in the nanoscale, in, State University of New York at Buffalo, 2016.

[94] S. Ashraf, B. Pelaz, P. del Pino, M. Carril, A. Escudero, W.J. Parak, M.G. Soliman, Q. Zhang, C. Carrillo-Carrion, Gold-based nanomaterials for applications in nanomedicine, in: Light-Responsive Nanostructured Systems for Applications in Nanomedicine, Springer, 2016, pp. 169-202.

[95] Y. Xie, C. Zhao, Y. Zhao, S. Li, J. Rufo, S. Yang, F. Guo, T.J. Huang, Optoacoustic tweezers: a programmable, localized cell concentrator based on opto-thermally generated, acoustically activated, surface bubbles, Lab on a Chip, 13 (2013) 1772-1779.

[96] K.K. Shung, High frequency ultrasonic imaging, Journal of medical ultrasound, 17 (2009) 25-30.

[97] H. Wan, J. Yue, S. Zhu, T. Uno, X. Zhang, Q. Yang, K. Yu, G. Hong, J. Wang, L. Li, A bright organic NIR-II nanofluorophore for three-dimensional imaging into biological tissues, Nature communications, 9 (2018) 1-9.

[98] M.R. Ali, Y. Wu, M.A. El-Sayed, Gold-nanoparticle-assisted plasmonic photothermal therapy advances toward clinical application, The Journal of Physical Chemistry C, 123 (2019) 15375-15393.

[99] A. Shakeri-Zadeh, S.K. Kamrava, M. Farhadi, Z. Hajizarimi, S. Maleki, A. Ahmadi, A scientific paradigm for targeted nanophotothermolysis; the potential for nanosurgery of cancer, Lasers in medical science, 29 (2014) 847-853.

[100] O. Bozinov, Y. Yang ,M.F. Oertel, M.G. Neidert, P. Nakaji, Laser interstitial thermal therapy in gliomas, Cancer Letters, 474 (2020) 151-157.

[101] N. Montemurro, Y. Anania, F. Cagnazzo, P. Perrini, Survival outcomes in patients with recurrent glioblastoma treated with Laser Interstitial Thermal Therapy (LITT): A systematic review, Clinical Neurology and Neurosurgery, (2020) 105942.

[102] T.J. Vogl, R. Straub, K. Eichler, D. Woitaschek, M.G. Mack, Malignant liver tumors treated with MR imaging–guided laser-induced thermotherapy: experience with complications in 899 patients (2,520 lesions), Radiology, 225 (2002) 367-377.

[103] T. Vogl, M. Mack, R. Straub, K. Eichler, K. Engelmann, A. Roggan, S. Zangos, Percutaneous interstitial thermotherapy of malignant liver tumors, RoFo :Fortschritte auf dem Gebiete der Rontgenstrahlen und der Nuklearmedizin, 172 (2000) 12-22.

[104] H.-J. Schwarzmaier, F. Eickmeyer, W. von Tempelhoff, V.U. Fiedler, H. Niehoff, S.D. Ulrich, Q. Yang, F. Ulrich, MR-guided laser-induced interstitial thermotherapy of recurrent glioblastoma multiforme: preliminary results in 16 patients, European journal of radiology, 59 (2006) 208-215.

[105] A. Carpentier, R.J. McNichols, R.J. Stafford, J.P. Guichard, D. Reizine, S. Delaloge, E. Vicaut, D. Payen, A. Gowda, B .George, Laser thermal therapy: Real-time MRI-guided and computer-controlled procedures for metastatic brain tumors, Lasers in surgery and medicine, 43 (2011) 943-950.

[106] C. Rosenberg, R. Puls, K. Hegenscheid, J. Kuehn, T. Bollman, A. Westerholt, C. Weigel, N. Hosten, Laser ablation of metastatic lesions of the lung: long-term outcome, American Journal of Roentgenology, 192 (2009) 785-792.

[107] A. Hashemian, H. Eshghi, G. Mansoori, A. Shakeri-Zadeh, A. Mehdizadeh, Folate-conjugated gold nanoparticles (synthesis, characterization and design for cancer cells nanotechnology-based targeting), International Journal of Nanoscience and Nanotechnology, 5 (2009) 25-34.

[108] A. Shakeri-Zadeh, H. Eshghi, G. Mansoori, A. Hashemian, Gold nanoparticles conjugated with folic acid using mercaptohexanol as the linker, Journal Nanotechnology Progress International, 1 (2009) 1-44.

[109] E. Zeinizade, M. Tabei, A. Shakeri-Zadeh, H. Ghaznavi, N. Attaran, A. Komeili, B. Ghalandari, S. Maleki, S.K. Kamrava, Selective apoptosis induction in cancer cells using folate-conjugated gold nanoparticles and controlling the laser irradiation conditions, Artificial cells, nanomedicine, and biotechnology, 46 (2018) 1026-1038.

[110] V. Hosseini, M. Mirrahimi, A. Shakeri-Zadeh, F. Koosha, B. Ghalandari, S. Maleki, A. Komeili, S.K. Kamrava, Multimodal cancer cell therapy using Au@Fe2O3 core–shell nanoparticles in combination with photo-thermo-radiotherapy, Photodiagnosis and photodynamic therapy, 24 (2018) 129-135.

[111] Z. Abed, J. Beik, S. Laurent, N. Eslahi, T. Khani, E.S. Davani, H. Ghaznavi, A. Shakeri-Zadeh, Iron oxide–gold core–shell nano-theranostic for magnetically targeted photothermal therapy under magnetic resonance imaging guidance, Journal of cancer research and clinical oncology, 145 (2019) 1213-1219.

[112] J. Beik, M. Asadi, S. Khoei, S. Laurent, Z. Abed, M. Mirrahimi, A. Farashahi, R. Hashemian, H. Ghaznavi, A. Shakeri-Zadeh, Simulation-guided photothermal therapy using MRI-traceable iron oxide-gold nanoparticle, Journal of Photochemistry and Photobiology B: Biology, 199 (2019) 111599.

[113] M. Mirrahimi, J. Beik, M. Mirrahimi, Z. Alamzadeh, S. Teymouri, V.P. Mahabadi, N. Eslahi, F. Ebrahimi, H. Ghaznavi, A. Shakeri-Zadeh, Triple combination of heat, drug and radiation using alginate hydrogel co-loaded with gold nanoparticles and cisplatin for locally synergistic cancer therapy, International Journal of Biological Macromolecules, 158 (2020) 617.

[114] Z. Alamzadeh, J. Beik, M. Mirrahimi, A. Shakeri-Zadeh, F. Ebrahimi, A .Komeili, B. Ghalandari, H. Ghaznavi, S.K. Kamrava, C. Moustakis, Gold nanoparticles promote a multimodal synergistic cancer therapy strategy by co-delivery of thermo-chemo-radio therapy, European Journal of Pharmaceutical Sciences, 145 (2020) 105235.

[115] S.C. Gad, K.L. Sharp, C. Montgomery, J.D. Payne, G.P. Goodrich, Evaluation of the toxicity of intravenous delivery of auroshell particles (gold–silica nanoshells), International journal of toxicology, 31 (2012) 584-594.

[116] J.M. Stern, V.V. Kibanov Solomonov, E. Sazykina, J.A. Schwartz, S.C. Gad, G.P. Goodrich, Initial evaluation of the safety of nanoshell-directed photothermal therapy in the treatment of prostate disease, International journal of toxicology, 35 (2016) 38-46.

[117] D.A. Winkler, E .Mombelli, A. Pietroiusti, L. Tran, A. Worth, B. Fadeel, M.J. McCall, Applying quantitative structure–activity relationship approaches to nanotoxicology: current status and future potential, Toxicology, 313 (2013) 15-23.

[118] T. Puzyn, B. Rasulev, A. Gajewicz, X. Hu, T.P. Dasari, A. Michalkova, H.-M. Hwang, A. Toropov, D. Leszczynska, J. Leszczynski, Using nano-QSAR to predict the cytotoxicity of metal oxide nanoparticles, Nature nanotechnology, 6 (2011) 175-178.

[119] Y. Huang, X. Li, S. Xu, H. Zheng, L .Zhang, J. Chen, H. Hong, R. Kusko, R. Li, Quantitative Structure–Activity Relationship Models for Predicting Inflammatory Potential of Metal Oxide Nanoparticles, Environmental Health Perspectives, 128 (2020) 067010.

[120] Y. Gao, H. Zhai, X. She, H. Si ,Quantitative Structure-activity Relationships; Studying the Toxicity of Metal Nanoparticles, Current Topics in Medicinal Chemistry, 20 (2020) 2506-2517.

[121] H. Baharifar, A. Amani, Cytotoxicity of chitosan/streptokinase nanoparticles as a function of size: an artificial neural networks study, Nanomedicine: Nanotechnology, Biology and Medicine, 12 (2016) 171-180.

[122] R. Concu, V.V. Kleandrova, A. Speck-Planche, M.N.D. Cordeiro, Probing the toxicity of nanoparticles: a unified in silico machine learning model based on perturbation theory, Nanotoxicology, 11 (2017) 891-906.

[123] A. Amani, D. Mohammadyani, Artificial neural networks: applications in nanotechnology, in: Artificial neural networks—application, INTECH, Rijeka, 2011.

[124] A. Amani, P. York ,H. Chrystyn, B.J. Clark, D.Q. Do, Determination of factors controlling the particle size in nanoemulsions using Artificial Neural Networks, European Journal of Pharmaceutical Sciences, 35 (2008) 42-51.

Journal Pre-proof